Applied Microbiology and Biotechnology (2024) 108:540
https://doi.org/10.1007/s00253-024-13364-3

MINI-REVIEW

Understanding microbial syngas fermentation rates

Iris Kerkhof[1] · **Lars Puiman**[1] · **Adrie J. J. Straathof**[1]

Received: 18 September 2024 / Revised: 19 November 2024 / Accepted: 20 November 2024 / Published online: 20 December 2024

Abstract

Syngas fermentation to ethanol has reached industrial production. Further improvement of this process would be aided by quantitative understanding of the influence of imposed reaction conditions on the fermentation performance. That requires a reliable model of the microbial kinetics. Data were collected from 37 steady states in chemostats and from many batch experiments that use *Clostridium authoethanogenum*. Biomass-specific rates from CO conversion experiments were related to each other according to simple reaction stoichiometries and the Pirt equation, with only the ratio of ethanol to acetate production remaining as degree of freedom. No clear dependency of this ratio on dissolved concentrations, such as CO or acetic acid concentration, was found. This is largely caused by the lack of knowledge about the dependency of the CO uptake rate (and hence all other rates) on the CO concentration. This knowledge gap is caused by a lack of dissolved CO measurements. For dissolved H_2, a similar gap applies. Modelling H_2 consumption adds more degrees of freedom to the system, so that more structured experiments with H_2 is needed. The inhibition of gas consumption by acetate and ethanol is partly known but needs further study.

Key points

- *Set of Clostridium autoethanogenum syngas fermentation data from chemostats.*
- *Unstructured kinetic models can relate most biomass-specific rates to dilution rates.*
- *Lack of dissolved gas measurements limits deeper understanding.*

Keywords *Clostridium autoethanogenum* · Chemostats · Kinetic model · Syngas · Carbon monoxide · Fermentation

Symbols

a	Specific interfacial area, m^2/m^3
c	Concentration, mol/L or g/L
c^*	Solubility, mol/L
D	Liquid dilution rate, h^{-1}
D_L	Diffusivity constant, m^2/s
H	Henry constant, mol/(m^3 Pa)
k_L	Mass transfer coefficient, m/h
$k_L a$	Volumetric mass transfer coefficient, h^{-1}
K_s	Affinity constant, mol/L
K_I	Inhibition constant, mol/L
m	Maintenance requirement, mol/(g_{DW} h)
p	Pressure, Pa
q	Biomass-specific rate, mol/(g_{DW} h)
T	Temperature, K
T_N	Gas–liquid transfer rate, mol/h
V_L	Liquid broth volume, m^3
y	Mole fraction, mol/mol$_{gas}$
$Y_{i/j}$	Yield, mol$_i$/mol$_j$
μ	Biomass-specific growth rate, h^{-1}

Superscripts and subscripts

0	Base value
AcT	Total acetate
BDO	2,3-Butanediol
DW	Dry weight (biomass)
EtOH	Ethanol
HAc	Acetic acid
i	Species i
L	Liquid phase
max	Maximum
out	In the outflow
R	Reaction
s	Substrate
x	Dry biomass on 1 C formula basis

✉ Adrie J. J. Straathof
a.j.j.straathof@tudelft.nl

[1] Department of Biotechnology, Delft University of Technology, van der Maasweg 9, 2629 HZ Delft, The Netherlands

Introduction

Mixtures of CO, H_2, and CO_2 are collectively called syngas. Traditionally, they are produced from fossil resources or waste-streams. Novel production methods, which are potentially more sustainable, use gasification of biomass or municipal waste and electroreduction of CO_2 and water (Bachmann et al. 2023; Detz et al. 2024). Conversion of syngas to useful products could contribute to a circular economy.

Acetogenic bacteria can anaerobically grow on syngas, leading to interesting metabolic product such as acetate (acetogenesis) and ethanol (solventogenesis). Especially, the gas fermentation model organism *Clostridium autoethanogenum* stands out as a robust and versatile platform for gas fermentation, being already used in industrial processes for producing ethanol (Liew et al. 2016) and being developed for many other products. Minor natural products of *C. autoethanogenum* are 2,3-butanediol and lactate (Köpke et al. 2014), and after metabolic engineering, it has produced other useful compounds such as acetone and isopropanol (Liew et al. 2022), ethylene glycol (Dang et al. 2021), ethyl acetate (Dykstra et al. 2022), and poly-3-hydroxybutyrate (de Souza Pinto Lemgruber et al. 2019).

Because of increasing commercial and scientific interest, the literature on anaerobic syngas fermentation by *C. autoethanogenum* and many other acetogenic bacteria is expanding rapidly. Many recent reviews have treated the bacteria, strain engineering, bioenergetics, growth nutrients and inhibitors, fermentation operation, process strategies, and commercialization (Bae et al. 2022; Elisiário et al. 2022; Fackler et al. 2021; Fernández-Blanco et al. 2023; Katsyv and Müller 2020; Khalid et al. 2024; Kim et al. 2023; Köpke and Simpson 2020; Owoade et al. 2023; Stoll et al. 2020; Yang et al. 2021). However, no systematic attention has been given to the status of knowledge on the microbial kinetics, even though such knowledge is a central aspect in this field. For rational optimization of the design and operation of syngas bioreactors, predictive kinetic models are crucial. These need to be obtained from lab-scale experiments, since industrial experimentation is too expensive. It is known how to combine lab-scale microbial kinetics with computational fluid dynamics to predict industrial-scale performance (Puiman et al. 2024), but the models used for lab-scale microbial kinetics still have large degrees of uncertainty, as will be shown in this review.

The microbial kinetics depend on factors that have been varied widely, namely all fermentation operation conditions including the used microbial strain. Not all these conditions will be elaborated here. The focus will be on the influence of concentrations of extracellular substrates and products on their rate of consumption and production by wild-type *C. autoethanogenum*. Deeper knowledge of these kinetics will facilitate the design of syngas fermentation processes for producing acetate and ethanol. To minimize the number of unknown parameters, established kinetic models will be used, which has been useful in many cases (Heijnen and Kleerebezem 2010).

As we will focus on basic models, intracellular kinetics will not be addressed. These add another layer of complexity and require additional degrees of freedom, but that is especially useful for finding targets for metabolic engineering (van Rosmalen et al. 2022).

Kinetic data from chemostats

Syngas fermentation experiments have been done in different operation modes. Batch operation often applies to both gas phase and liquid phase in flasks and other small devices. In bioreactors, gas inflow and outflow are always continuous, like air flow in aerobic fermentations, but the aqueous liquid can be provided at once (batch operation) or continuous (chemostat, if a steady state is obtained). In some cases, cell retention devices have been used with chemostats (Perret et al. 2024; Richter et al. 2013), or cell-retaining membrane reactors are used (Elisiário et al. 2022), but these complicate kinetic studies because it will become important to monitor cell death.

Chemostats are a very useful research tool for traditional carbohydrate fermentation but are hardly applied in industry (Heijnen et al. 1992). However, industrial syngas fermentation to ethanol uses chemostats (Fackler et al. 2021), because none of the constraints mentioned by Heijnen et al. (1992) applies:

- The used syngas bacteria will not be outcompeted by mutants or by microbes entering as contamination, because selective conditions are imposed at which microbes grow most efficiently on syngas by catabolizing it to ethanol.
- The substrate feed concentration will not constrain the product concentration in the liquid phase, because substrate supply is via gas transfer, decoupled from the liquid inflow rate.
- The ethanol market is huge, with small economic margins, pushing the process to large-scale continuous operation with no or low storage of gaseous feed.

Kinetic data from industrial chemostats are scarce, but many lab-scale chemostat data for *C. autoethanogenum* have become available recently. Tables 1 and 2 show 37 steady-state data sets that we gathered. Lately, additional data have been published for six evolved strains (Ingelman

Table 1 Operating conditions for *C. autoethanogenum* chemostats in steady state (SST). All were at 37 °C and 1 atm. For additional data, see Online Resource 1

SST	Reference	Strain	pH	D (d^{-1})	Gas in (vvm)	CO in (atm)	H_2 in (atm)	CO_2 in (atm)	inert in (atm)	Stirring (min^{-1})
1	Heffernan et al. (2020)	DSM 19630	5	0.10	0.04	0.02	0.65	0.23	0.1	1200
2			5	0.47	0.043	0	0.67	0.23	0.1	500
3			5	0.50	0.04	0.02	0.65	0.23	0.1	800
4	Valgepea et al. (2018)	DSM 19630	5	1.0	0.062	0.6	0	0	0.4	510
5			5	1.0	0.062	0.6	0	0	0.4	665
6			5	1.0	0.062	0.15	0.45	0	0.4	650
7			5	1.0	0.15	0.15	0.45	0	0.4	1000
8	Valgepea et al. (2017a)	DSM 19630	5	0.96	0.062	0.5	0.2	0.2	0.1	500
9			5	0.96	0.062	0.5	0.2	0.2	0.1	500
10			5	0.96	0.062	0.5	0.2	0.2	0.1	590
11			5	0.96	0.062	0.5	0.2	0.2	0.1	650
12			5	0.96	0.062	0.5	0.2	0.2	0.1	650
13	de Lima et al. (2022)	DSM 23693	5	1.03	0.067	0.6	0	0	0.4	690
14			5	2.03	0.096	0.6	0	0	0.4	815
15			5	2.79	0.096	0.6	0	0	0.4	1175
16			5	1.01	0.067	0.5	0.2	0.2	0.1	675
17			5	2.01	0.096	0.5	0.2	0.2	0.1	800
18			5	2.79	0.096	0.5	0.2	0.2	0.1	1160
19	Elisiário et al. (2023)	DSM 10061	5.9	0.21	0.01	0.5	0	0	0.5	500
20			5.9	0.58	0.01	0.5	0	0	0.5	500
21			5.9	0.94	0.01	0.5	0	0	0.5	500
22			5.9	0.96 [a]	0.01	0.5	0	0	0.5	500
23	Allaart (2023)	DSM 10061	5.5	0.24	0.062	0.1	0	0	0.9	600
24			5.5	0.24	0.062	0.1	0	0	0.9	600
25	Chen et al. (2012)	DSM10061	5	1.5	0.19	0.5	0	0.2	0.3	0 [b]
26			5	1.5	0.23	0.5	0	0.2	0.3	0 [b]
27			5	1.5	0.27	0.5	0	0.2	0.3	0 [b]
28	Diender (2019)	DSM10061	6.2	0.67	0.0040	0.66	0	0	0.34	400
29			6.2	0.67	0.0040	0.66	0	0	0.34	400
30			6.2	0.5	0.0020	1	0	0	0	400
31			6.2	0.5	0.0024	0.83	0.17	0	0	400
32			6.2	0.5	0.0028	0.71	0.29	0	0	400
33			6.2	0.5	0.0035	0.56	0.44	0	0	400
34			6.2	0.67	0.0040	0.66	0	0	0.34	400
35			6.2	0.67 [a]	0.0040	0.66	0	0	0.34	400
36			6.2	0.67 [a]	0.0040	0.66	0	0	0.34	400
37			6.2	0.67 [a]	0.0040	0.66	0	0	0.34	400

[a]AcT was added to liquid inflow: 10.15, 1.50, 3.00, and 5.40 g/L for SST 22, 35, 36, and 37, respectively

[b]Bubble column with fast liquid recycling

et al. 2024), but here, the focus will be on wild-type strains. The included data cover a wide range of liquid dilution rates (D), gas inflow rates (in vvm, volume gas per volume liquid per minute), and gas compositions. Three different *C. autoethanogenum* strains were used, and somewhat different micronutrients and pH control agents were supplied. Ammonia was nitrogen source, although Elisiário et al. (2023) used some yeast extract in addition. For comparison of these steady states, we will neglect differences between strains and media, except for differences in setpoint pH. Furthermore, hydrodynamics differed per reference not only because of different gas supply rates and stirring rates as shown in Table 1, but also because of different types of bioreactors, spargers, and stirrers, which were not always reported in detail but sometimes available from manuals of the suppliers (see Online Resource 1).

Steady-state measurements include the flow rates, the gas fractions, and the concentrations of dry biomass (X), ethanol (EtOH), total acetate (AcT, which is the sum of undissociated acetic acid and acetate anion), and 2,3-butanediol (BDO). The references cited in Table 1 all mention the biomass-specific production rates q_i ($mol_i/(mol_x\ h)$) including the specific growth rate μ (h^{-1}) such as calculated from the measured data. All rates are expressed here as production rates, implying that negative rates are consumption rates. For compound i, volume-specific production rates r_i (mol_i per liquid volume per time) will be proportional to dry biomass concentration c_x, (mol_x per liquid volume) such that using biomass-specific production rates q_i is convenient.

When evaluating steady-state data, it is good practice to assess the quality of the data through the carbon balances (Eq. 1) and electron balances (Eq. 2). Taking $CH_{1.52}O_{0.46}N_{0.28}S_{0.0059}P_{0.042}$ as one-carbon biomass formula (Norman et al. 2019), these become:

$$q_{CO} + q_{CO_2} + \mu + 2q_{AcT} + 2q_{EtOH} + 4q_{BDO} = 0 \quad (1)$$

$$2\boldsymbol{q_{H_2}} + 2\boldsymbol{q_{CO}} + 3.76\boldsymbol{\mu} + 8\boldsymbol{q_{AcT}} + 12\boldsymbol{q_{EtOH}} + 22\boldsymbol{q_{BDO}} = 0 \quad (2)$$

Typically, gaps of less than 10% in these balances were found (Fig. 1), which indicates good quality data. Still, the gaps are an issue when modelling the kinetics. No kinetic model can close gaps in carbon or electron balances, and kinetic model selection may become very dependent on the choice of the output variable that is fitted. Data reconciliation may be used on basis of the perceived error ranges of the input variables and measured variables (Lange and Heijnen 2001). For the steady states mentioned, data reconciliation led to closed balances (Fig. 1), and a set of reconciled data that had generally small differences with the published data (See Online Resource 1 and (Kerkhof 2024)). Table 2 mentions the key reconciled data that will be used for further analysis in the next sections. Online Resource 1 mentions also the originally reported data and all assumed standard deviations.

The q-values in Table 2 confirm trends that have been reported by the authors who produced the underlying data: CO and H_2 are partly consumed when supplied. If H_2 is not supplied, it is produced in traces using electrons from CO when the pH is 5. Acetate and (in case of pH 5) ethanol are the main products, while 2,3-butanediol (BDO) is a minor product. CO_2 is generally co-produced, but co-consumed in case that much more H_2 than CO is available.

Stoichiometry of catabolic reactions

Before moving to kinetic models for describing the steady-state data, basic features of the metabolic pathways used by *C. autoethanogenum* will be summarized. This can provide a mechanistic basis to a kinetic description, which is more likely to lead to understanding and more useful than empirical descriptions for extrapolation beyond conditions that have been studied.

C. autoethanogenum uses the Wood-Ljungdahl pathway to convert syngas into acetyl-CoA (Ljungdhal 1986; Sun et al. 2019; Wood 1991). During catabolism, acetyl-CoA is reduced to fermentation products, mainly acetate and ethanol, while simultaneously generating ATP for cellular growth and maintenance (Liew et al. 2016; Sun et al. 2019). Ethanol can be produced directly via acetyl-CoA or indirectly, using acetate as a precursor (Fig. 2). In the direct route, acetyl-CoA is converted into ethanol via acetaldehyde by two alcohol dehydrogenases (ADH). In the indirect route, acetyl-CoA is initially converted into acetate. Next, acetate is reduced by aldehyde:ferredoxin oxidoreductase (AOR) and ADH into ethanol.

Through knockout studies and metabolomic analysis, it has been demonstrated that the indirect pathway is the preferred route for ethanol production by *C. autoethanogenum* (Diender 2019; Liew et al. 2017; Valgepea et al. 2017a). Therefore, when focusing on CO as substrate, the catabolism can be represented by two catabolic reactions, namely the production of acetate from CO through reaction R1, shown in Eq. (3), and the production of ethanol from acetate through reaction R2, shown in Eq. (4). Summing these two catabolic reactions yields the reaction for ethanol from CO (R3), shown in Eq. (5). As catabolic reaction R3 is the sum of catabolic reactions R1 and R2, it usually does not need to be discussed separately.

$$R1\ \ 4\ CO + 2\ H_2O \rightarrow\ AcT + 2\ CO_2 + Y_{ATP,R1}\ ATP \quad (3)$$

$$R2\ \ 2\ CO + AcT + H_2O\ \rightarrow\ EtOH + 2\ CO_2 + Y_{ATP,R2}\ ATP \quad (4)$$

Table 2 Key reconciled data for the steady states of Table 1. For additional data, see Online Resource 1

SST	Gas mole fraction out [-]			Gas outflow [vvm]	q [mmol/(g_x/h)]						μ [h^{-1}]	c [g/L]			
	CO	H_2	CO_2		CO	H_2	CO_2	EtOH	AcT	BDO		EtOH	AcT	BDO	X
1	0.015	0.582	0.188	0.0186	−3.73	−109.7	−41.17	11.90	9.75	0.000	0.042	4.42	4.73	0.00	0.34
2	0.0	0.663	0.222	0.0374	0.00	−52.19	−20.70	5.44	4.53	0.000	0.020	2.28	2.47	0.00	0.18
3	0.023	0.581	0.201	0.0205	−1.52	−64.38	−23.22	8.25	3.72	0.000	0.021	9.63	5.65	0.00	0.54
4	0.542	0.002	0.043	0.0601	−24.06	0.58	13.53	1.31	3.17	0.000	0.042	0.68	2.16	0.00	0.47
5	0.336	0.005	0.204	0.0545	−33.76	0.46	19.88	2.75	3.25	0.074	0.042	4.17	6.43	0.22	1.37
6	0.099	0.415	0.008	0.0518	−23.29	−35.94	2.21	8.63	1.12	0.000	0.042	4.16	0.70	0.00	0.44
7	0.069	0.415	0.022	0.1185	−24.78	−30.22	4.57	7.39	1.92	0.000	0.042	11.08	3.75	0.00	1.37
8	0.477	0.177	0.236	0.0567	−21.80	−12.97	5.52	1.20	6.18	0.000	0.040	0.61	4.13	0.00	0.45
9	0.474	0.176	0.240	0.0563	−20.76	−12.16	5.41	1.20	5.72	0.000	0.040	0.70	4.33	0.00	0.51
10	0.402	0.137	0.334	0.0489	−25.50	−12.77	8.76	2.47	5.11	0.010	0.040	3.10	8.34	0.02	1.09
11	0.315	0.126	0.424	0.0458	−30.94	−12.35	13.08	3.74	4.25	0.090	0.040	5.63	8.34	0.27	1.31
12	0.311	0.124	0.429	0.0456	−29.67	−11.88	12.64	3.70	3.87	0.091	0.040	5.90	8.02	0.28	1.39
13	0.306	0.003	0.227	0.0575	−34.89	0.28	20.31	2.70	3.63	0.074	0.043	4.61	8.07	0.25	1.57
14	0.247	0.002	0.278	0.0812	−55.07	0.25	33.13	5.33	3.57	0.225	0.085	4.85	4.24	0.40	1.67
15	0.140	0.002	0.360	0.0771	−69.45	0.28	41.13	6.32	5.36	0.135	0.116	4.14	4.57	0.17	1.65
16	0.321	0.159	0.393	0.0523	−25.74	−7.83	11.26	2.24	3.99	0.104	0.042	3.84	8.93	0.35	1.57
17	0.194	0.104	0.554	0.0645	−55.42	−19.54	25.82	7.55	4.96	0.346	0.084	6.49	5.56	0.58	1.57
18	0.122	0.124	0.605	0.0648	−68.53	−19.03	34.24	8.79	4.85	0.645	0.117	4.98	3.59	0.72	1.43
19	0.171	0.000	0.228	0.0083	−16.22	0.00	8.61	0.36	3.07	0.104	0.009	1.02	11.3	0.58	0.54
20	0.118	0.000	0.256	0.0080	−20.77	0.00	10.45	0.07	4.56	0.039	0.024	0.06	5.45	0.07	0.48
21	0.130	0.000	0.247	0.0080	−26.77	0.00	13.41	0.11	5.83	0.000	0.039	0.05	3.25	0.00	0.36
22	0.264	0.000	0.166	0.0088	−24.41	0.00	13.21	1.10	3.74	0.000	0.040	0.34	11.7	0.00	0.27
23	0.064	0.001	0.020	0.0615	−10.87	0.36	5.81	0.22	2.12	0.000	0.010	0.53	6.62	0.00	0.52
24	0.064	0.000	0.019	0.0614	−9.57	0.00	4.92	0.16	1.97	0.000	0.010	0.45	6.99	0.00	0.59
25	0.248	0.000	0.413	0.1703	−37.00	0.00	21.87	3.37	2.82	0.092	0.063	8.87	9.66	0.47	3.57
26	0.251	0.000	0.412	0.2056	−39.45	0.00	23.86	4.04	2.25	0.155	0.063	11.79	8.55	0.89	3.96
27	0.266	0.000	0.401	0.2421	−38.37	0.00	23.56	4.30	1.63	0.145	0.063	14.21	7.00	0.94	4.49
28	0.000	0.000	0.496	0.0026	−12.98	0.00	6.44	0.02	2.72	0.000	0.028	0.014	2.94	0.00	0.50
29	0.125	0.000	0.402	0.0028	−14.12	0.00	7.00	0.00	3.03	0.000	0.028	0.000	2.60	0.00	6.40
30	0.000	0.000	1.000	0.0010	−17.64	0.00	8.79	0.01	4.02	0.000	0.021	0.009	3.22	0.00	0.28
31	0.137	0.026	0.837	0.0009	−20.64	−4.10	8.24	0.02	5.79	0.000	0.021	0.009	3.66	0.00	0.22
32	0.185	0.120	0.695	0.0008	−18.53	−7.14	5.68	0.03	5.99	0.000	0.021	0.018	4.16	0.00	0.24
33	0.147	0.317	0.537	0.0005	−15.51	−11.57	2.34	0.42	5.77	0.000	0.021	0.276	4.96	0.00	0.30
34	0.220	0.000	0.332	0.0030	−32.34	0.00	16.11	0.00	7.59	0.000	0.028	0.000	2.46	0.00	0.15
35	0.256	0.000	0.305	0.0030	−33.71	0.00	16.83	0.04	7.88	0.000	0.028	0.008	3.80	0.00	0.14
36	0.296	0.000	0.276	0.0031	−46.29	0.00	23.25	0.17	10.8	0.000	0.028	0.025	5.12	0.00	0.09
37	0.277	0.000	0.292	0.0031	−57.91	0.00	29.32	0.43	13.3	0.000	0.028	0.054	7.57	0.00	0.08

$$R3\ \ 6\,CO + 3H_2O \rightarrow EtOH + 4\,CO_2 + Y_{ATP,R3}\,ATP \qquad (5)$$

During growth on CO, production of BDO and H_2 is not specified or low compared to production of ethanol and acetate and therefore not elaborated on when discussing the microbial rate. Thus, the catabolism of CO is summarized in Fig. 3.

Both R1 and R2 need reducing equivalents that are obtained from CO via cofactors not shown in Fig. 2 (Katsyv and Müller 2020). ATP is produced in R1 and R2 through substrate level phosphorylation and chemiosmotic ion gradient-drive phosphorylation. In *C. autoethanogenum*, an Rnf complex generates this gradient, known as the proton motive force (PMF), by facilitating proton translocation across the membrane. Subsequently, the PMF drives ATP synthesis through the membrane-bound ATP synthase (Liew et al. 2016). Since the Wood-Ljungdahl pathway does not result in net production of ATP, *C. autoethanogenum* relies on chemiosmotic

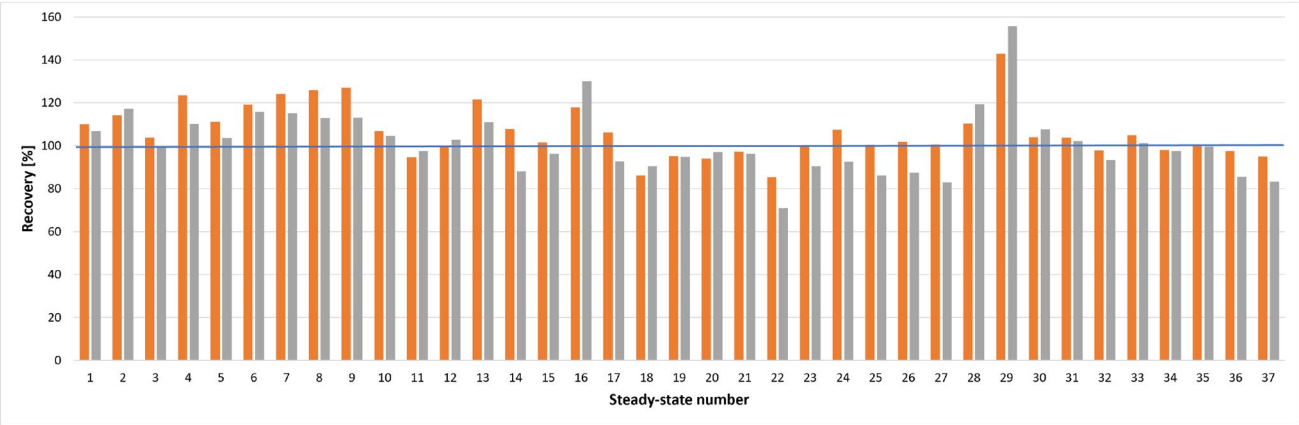

Fig. 1 Carbon recoveries (orange bars) and electron recoveries (grey bars) before data reconciliation for the 37 steady-state syngas fermentations. The horizontal blue line indicates 100% recovery in all cases after reconciliation. For details, see Kerkhof (2024)

energy conservation to conserve energy (Fernández-Blanco et al. 2023; Schuchmann and Müller 2014).

Using this knowledge, Katsyv and Müller (2020) reported ATP yields for catabolic reactions R1 ($Y_{ATP,R1}$) and R3 ($Y_{ATP,R3}$) of 1.5 mol_{ATP}/mol_{R1} and 2.4 mol_{ATP}/mol_{R3}, respectively, assuming the membrane-bound ATP synthase (ATPase) having an H^+/ATP-ratio of 3.6 and the methylene-THF reductase being electron bifurcating. The used H^+/ATP-ratio still needs proof (Mock et al. 2015) but electron bifurcation by methylene-THF reductase is in line with date from Munoz and Philips (2023). Because catabolic reaction R2 is the difference between R3 and R1, it can be

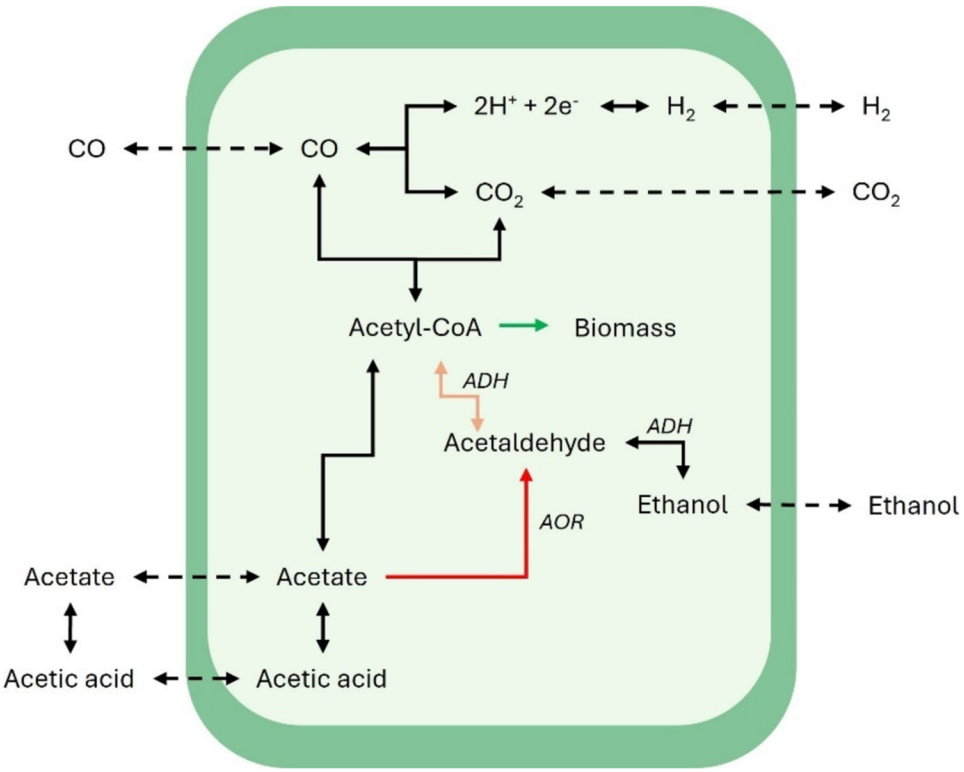

Fig. 2 Schematic representation of the pathways for ethanol production. In the direct pathway (orange), acetyl-CoA is converted into ethanol via acetaldehyde by alcohol dehydrogenase (ADH). Ethanol production via the indirect pathway (red) involves reduction of acetate into acetaldehyde by aldehyde:ferredoxin oxidoreductase (AOR)

deduced that the ATP yield for reaction R2 ($Y_{ATP,R2}$) would be 2.4 - 1.5 = 0.9 mol_{ATP}/mol_{R2}.

However, Norman et al. (2019) and Allaart et al. (2023) reported $Y_{ATP,R1}$, $Y_{ATP,R2}$, and $Y_{ATP,R3}$ values of 1.5, 0.6, and 2.1 mol_{ATP}/mol_{R}, respectively. We also found these ATP yield values when using the assumptions of Katsyv and Müller (2020) (see (Kerkhof 2024)). Following our ATP yields, the ATP yields per CO for reactions R1, R2, and R3 are 0.375, 0.30, and 0.35 mol_{ATP}/mol_{CO}, respectively. According to these numbers, *C. autoethanogenum* should use reaction R1 rather than R2 when CO is limiting, because R1 generates most ATP per CO.

There are several explanations for the occurrence of R2. The HAc concentration might reach a level that leads to substantial ATP costs for maintenance, such that the cell should rather limit a further increase of the AcT concentration by AcT reduction into ethanol through catabolic reaction R2 (Elisiário et al. 2023; Valgepea et al. 2017a). Then, when CO is used for R2, less CO will be available for R1, and per CO, less ATP becomes available for growth. For *C. ljungdahlii*, Richter et al. (2016) argue that the enzymes required for R2 are always abundant and that R2 occurs as overflow reaction as soon as a critical concentration of HAc is obtained. In this case, thermodynamic constraints require a very low concentration of the reaction-intermediate acetaldehyde, such that $c_{HAc} > 1000\ c_{acetaldehyde}$ (Liu et al. 2020). Allaart et al. (2023) claim that also *C. autoethanogenum* uses R2 as overflow mechanism if CO availability is not limiting. They mention that R2 needs much less enzymatic steps than R1, thus less enzymatic machinery, which is an advantage if the biology is rate-limiting.

In any case, AcT needs to be produced by R1 or needs to be added to be available for R2. To improve understanding, the dependencies of R1 and R2 on the concentrations of CO and AcT will be quantitatively discussed in later sections.

Incorporation of ATP production and consumption in growth kinetics

The ATP generated by the bacteria during catabolism by R1 and R2 is used for cell growth and non-growth-related processes (maintenance) (Heijnen and Kleerebezem 2010). This is represented by Eq. (6), with q_R as catabolic reaction rate in mol/(g $_{DW}$ h), $Y_{ATP,R}$ as ATP yield for catabolic reaction R in mol_{ATP}/mol, $Y^{max}_{x/ATP}$ as the maximum biomass yield per ATP in g $_{DW}/mol_{ATP}$, and m_{ATP} as the ATP required for maintenance in $mol_{ATP}/(g_{DW}\ h)$.

$$q_{R1}Y_{ATP,R1} + q_{R2}Y_{ATP,R2} = \frac{1}{Y^{max}_{x/ATP}}\mu + m_{ATP} \quad (6)$$

As acetate is the precursor of ethanol, q_{R1} is the sum of the observed total acetate production rate (q_{AcT}) and the observed ethanol production rate (q_{EtOH}). Ethanol is not further converted into other products, such that q_{R2} equals q_{EtOH}. Fitting of Eq. (6) to the *C. autoethanogenum* *q*-data for CO conversion obtained from Table 2 led to a slope of $Y^{max}_{x/ATP} = 6.36$ g $_{DW}/mol_{ATP}$ and an intercept of $m_{ATP} = 2.61\ mmol_{ATP}/(g_{DW}\ h)$. The fit shown in Fig. 4 contains no large deviation between experiments and model except for some of the data points of Diender (2019) that also showed relatively large mass balance gaps.

Valgepea et al. (2017b) assumed $Y_{x/ATP} = 21.3$ g $_{DW}/mol_{ATP}$ and $m_{ATP} = 8.4\ mmol_{ATP}/(g_{DW}\ h)$ on basis of a literature study on *Clostridial* bacteria grown on glucose. Valgepea et al. (2017a) calculated $m_{ATP} = 5.7$ and 7.4 $mmol_{ATP}/(g_{DW}\ h)$ at low and high biomass concentration, respectively, and assumed the difference to be caused by high acetate concentrations. In any case, these literature values are much larger than our values.

Our parameters imply that more ATP is used for growth than for maintenance if μ exceeds 0.0166 h^{-1}, which is the case for 80% of the steady states considered in Fig. 4. Yet, in none of these steady states, less than 10% of ATP is used for maintenance.

When taking Eq. (6) with the fitted and assumed parameter values for $Y_{ATP,R1}$, $Y_{ATP,R2}$, $Y_{x/ATP}$, and m_{ATP}, imposing growth rate μ (by choosing D) does not yet predict the individual values of q_{R1} and q_{R2}, and consequently also not of q_{AcT} and q_{EtOH}.

The Pirt equation, Eq. (7), for substrate distribution between growth and maintenance (Heijnen and Kleerebezem 2010; Pirt 1965) would be expected to give a more scattered fit to reconciliated literature data of q_{CO} vs. μ, since the amounts of CO used for growth and maintenance should depend on the proportion between reactions R1 and R2, which will depend on other factors than μ.

$$-q_{CO} = \frac{1}{Y^{max}_{x/CO}}\mu + m_{CO} \quad (7)$$

When partially removing one of these factors, c_{HAc}, by taking out the steady states with acetate addition to the feed, Fig. 5 provides an acceptable fit, probably because $Y_{ATP,R1} = 0.375$ and $Y_{ATP,R2} = 0.30\ mol_{ATP}/mol_{CO}$ are not widely different. The fit yielded $Y^{max}_{x/CO} = 1.85 \pm 0.15$ g $_{DW}/mol$ and $m_{CO} = 6.4 \pm 2.2\ mmol/(g_{DW}\ h)$, which is in line with the values of Elisiário et al. (2023), $Y^{max}_{x/CO} = 1.87$ g $_{DW}/mol$ and

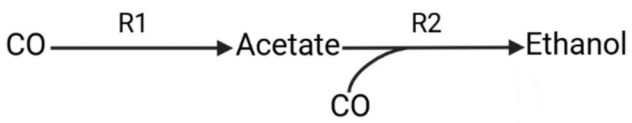

Fig. 3 Basic reaction scheme for CO conversion to ethanol

m_{CO} = 7.92 mmol/(g_{DW} h), who used a smaller dataset without reconciliation.

Determining dissolved syngas concentration

The microbial kinetics are expected to depend on the dissolved concentrations of the involved gases. However, *dissolved* concentrations of CO, H_2, and CO_2 have rarely been measured during syngas fermentation. Dissolved CO in stirred bioreactors has been measured off-line by using a reaction with myoglobin and spectroscopic analysis (Munasinghe and Khanal 2014; Ungerman and Heindel 2007). A Raman method was used for miniaturized reactors (Whang et al. 2022). Mann et al. (2021) developed an online system for CO measurement and used it during continuous stirred tank reactor cultivation of *Clostridium ljungdahlii* on CO. The measurement was done using a commercial CO sensor in the gas phase inside a silicon tube that was submerged in the bioreactor and was flushed with N_2 to obtain fast gas–liquid equilibration and gaseous CO concentrations in the applicable range.

The dissolved H_2 concentration of a syngas fermentation with *Clostridium carboxidivorans* was determined off-line by allowing liquid samples to equilibrate with a gas phase that was subsequently analyzed by GC (Munasinghe and Khanal 2014). However, the dissolved syngas concentrations were not used for explaining the intrinsic microbial kinetics.

If dissolved syngas concentrations have not been measured, but the gas composition has been measured, a model might be used to estimate dissolved concentrations c_i from gas compositions y_i. In case of gas–liquid equilibrium and ideal-mixing of both liquid and gas phase in the bioreactor, the dissolved concentration will equal the equilibrium concentration c_i*, which follows from a Henry relation:

$$c_i^* = p \cdot y_{i,out} \cdot H_i \tag{8}$$

The Henry coefficients H_i for water are known from literature and can be temperature-corrected (see (Kerkhof 2024)), while Eq. (8) accounts for correction to pressure p. The value of H_i will only slightly differ between water and fermentation broth.

However, assuming $c_i = c_i$* can easily lead to errors, even if fresh gas is supplied continuously. During batch fermentation with a continuous syngas flow and gas–liquid equilibrium, microbes typically start growing at a fixed value of μ until the amount of biomass has increased to a level where gas–liquid equilibration is not fast enough anymore to keep dissolved gas concentration at its equilibrium value, and the dissolved gas concentration becomes unknown.

During chemostat cultivation, gas–liquid equilibrium will rarely be valid for CO or H_2 while they are consumed by microbes. When choosing a medium that is rich in minor nutrients such as ammonia, the steady-state concentration of the microbes will increase up to a level where a gaseous substrate becomes limiting, such that Eq. (8) will not be valid. To calculate the dissolved gas concentrations (and subsequently the parameters of the microbial kinetics), the gas–liquid mass transfer equation is required (van 't Riet and Tramper 1991):

$$T_{N,i} = k_L a \cdot V_L \cdot \left(c_i^* - c_i\right) \tag{9}$$

Here, $T_{N,i}$ is the mole amount of gas i transferred from gas to liquid (with volume V_L), which can be derived from

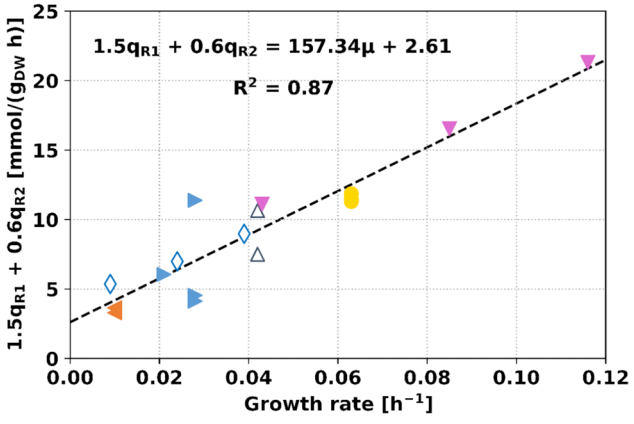

Fig. 4 Total ATP production in catabolic reactions R1 and R2 rate as function of the growth rate for CO fermentation by *C. autoethanogenum*. The line is the fit of Eq. (6) to the markers, which are reconciliated experimental data: open triangle (Valgepea et al. 2018); diamond (Elisiário et al. 2023); circle (Chen et al. 2018); pink downward arrow (de Lima et al. 2022); orange left arrow (Allaart 2023); blue right arrow (Diender 2019)

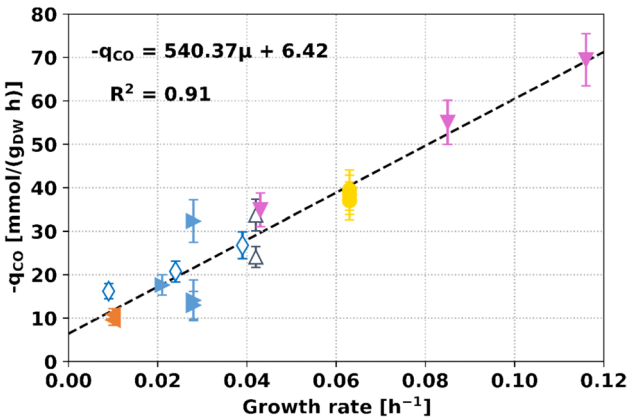

Fig. 5 Biomass-specific CO consumption of *C. autoethanogenum* as function of its growth rate. The line is the fit of Eq. (7) to reconciliated experimental data, indicated by the markers: open triangle (Valgepea et al. 2018); diamond (Elisiário et al. 2023); circle (Chen et al. 2018); pink down arrow (de Lima et al. 2022); orange left arrow (Allaart 2023); pink right arrow (Diender 2019)

measured gas inflow and outflow and their compositions. The liquid concentration c_i^* that is in equilibrium with the gas is obtained from Eq. (8). Now, the dissolved concentration c_i can be calculated from Eq. (9) when the gas transfer parameter k_La is known. This parameter consists of the volume-specific area a (m^2/m^3), which strongly depends on bioreactor operation conditions and broth composition, and rate constant k_L (m/s), which is compound-specific as can be indicted by using $k_{L,i}$. For O_2 in aerated water, k_La has been extensively measured for a large range of bioreactors, and correlative models have been formulated that allow prediction of $k_{L,O2}a$ for a specific bioreactor with a specific sparger, stirrer type, gas flow, and agitation rate (Garcia-Ochoa and Gomez 2009; van 't Riet and Tramper 1991).

One can recalculate this into k_La of the syngas components at the same condition, using diffusion coefficients D_L and absolute temperature T:

$$k_{L,i}a = k_{L,O_2}a \cdot 1.022^{T-293.15} \cdot \sqrt{\frac{D_{L,i}}{D_{L,O_2}}} \quad (10)$$

This usefulness of this approach depends on the reliability of the available correlations for $k_{L,O_2}a$. These have mostly been generated from experiments with dilute synthetic aqueous solutions. However, as mentioned, the broth composition has a large influence on k_La. The main cause is that solutes influence the surface tension gradient between the aqueous and gas phase, leading to large changes in bubble sizes, hence in the specific interfacial area a. For syngas fermentation broths, the concentration of a few g/L of ethanol makes a large difference on the bubble size, but also in the presence of salts, the biomass type and concentration influence both a and k_L (Puiman et al. 2022). Predictive models do not reliably include the influence of the broth composition on $k_{L,O_2}a$ (Volger et al. 2024).

Therefore, one might consider determining the k_La value of O_2 at the end of a chemostat steady-state measurement, after all sampling has been finished. One could do so by switching the syngas inflow to air inflow of the same rate and then measuring the appearance of dissolved O_2 according to the "dynamic method" with a common dissolved O_2 sensor (van 't Riet and Tramper 1991). Such a measurement will kill the strictly anaerobic acetogens and change the broth composition during the O_2 measurements. Continuing the syngas fermentation to a next steady-state condition, where k_La might be different again, will not be possible anymore.

For batch experiments, an approach to still obtain dissolved syngas concentrations from measured gas concentrations has been developed by Vega et al. (1989). For a series of fermentations at different CO pressures but similar hydrodynamics, the k_La/H_{CO} value was derived from late stages in the experiments, where c_{CO} could be assumed to be very much smaller than the CO concentration that would be at equilibrium with gas-phase concentrations. This assumption was correct due to fast CO conversion at high cell concentrations. Then, in the mass balance for dissolved CO in early stages of the fermentation, this k_La/H_{CO} value and known course of CO consumption rates from gas phase analysis were used, which provided the course of the dissolved CO concentration.

For dissolved H_2 measurements, the same might be done, but reports of anaerobic syngas fermentation with measurements of dissolved H_2 concentrations are rare (Morinaga and Kawada 1990). Dissolved CO_2 measurements are less critical. Since CO_2 dissolves about 40 times better than CO or H_2, it reaches gas–liquid equilibrium much easier, such that dissolved CO_2 concentrations may be reliably estimated from its partial gas pressure using Eq. (8) if the CO_2 fraction in the gas is not too low.

All aforementioned complications for CO and H_2 might be avoided if sensors would become available for measuring routinely and accurately the dissolved concentrations of CO and H_2 online when both are present during fermentation, comparable to how dissolved O_2 concentrations are routinely measured during aerobic fermentation and used for process optimization and control. Potential methods for CO and H_2 measurements have been reviewed by Dang et al. (2021). Limitations of online sensors are related to differentiation between CO and H_2, sensor reversibility, response time, and fermentation interference. Offline methods require laborious manual operations.

Influence of CO and H_2 on uptake kinetics and maximum growth rate

For the biomass-specific uptake rate of substate ($-q_s$, because q is defined as production rate), Eq. (11) is typically used because the uptake is assumed to hyperbolically approach a maximum rate (Heijnen and Kleerebezem 2010).

$$q_s = q_s^{max}\frac{c_s}{K_s + c_s} \quad (11)$$

However, high CO concentrations are generally considered to be inhibiting syngas fermentation, which has a molecular background at the level of the hydrogenase-formate dehydrogenase complex (Wang et al. 2013). Therefore, an additional substrate inhibition term as given in Eq. (12) has been proposed for the CO uptake rate (Vega et al. 1989). This is an empirical additional term, inspired by substrate inhibition description in enzyme kinetics. The kinetic parameters values of Eq. (12) such as determined from batch anaerobic growth experiments of *Peptostreptococcus productus* on CO (Vega et al. 1989) are given in

Table 3, together with similar data for other bacteria. The parameter values depend strongly on the microbe.

$$q_{CO} = q_{CO}^{max} \frac{c_{CO}}{K_{s,CO} + c_{CO} + \frac{(c_{CO})^2}{K_{I,CO}}} \quad (12)$$

We found no such kinetic studies for *C. autoethanogenum*, so it is not clear how its fermentation rate depends on CO concentration. To bypass this knowledge gap, Eq. (12) has been used with the parameter values from Table 3 of Mohammadi et al. (2014) for *C. ljungdahlii* to simulate syngas fermentation by the related *C. autoethanogenum* (Chen et al. 2018; Puiman et al. 2024).

Using the values of *C. ljungdahlii* (Table 3), the highest CO uptake rate can be expected at $c_{CO} = (K_{s,CO}K_{I,CO})^{0.5} = 0.11$ mmol/L, which is the dissolved concentration at equilibrium with 0.13 atm CO in the gas phase.

For H_2, with lack of syngas fermentation studies that report uptake rate determination, Eq. (11) has been used for process modelling, and it was argued that $K_{s,H2}$ = 0.04 mmol/L would be a reasonable value (Almeida Benalcázar et al. 2020). Later, Munoz and Philips (2023) found that at least 0.015 mmol/L H_2 needs to be dissolved before it can be consumed by *C. autoethanogenum* DSM 10061 at pH 7 from a H_2/CO_2 mixture, due to the low driving force for ATP generation by H_2. This suggests that Eq. (11) needs to be modified to account for that constraint. For other studied acetogens, H_2 thresholds were less critical (Munoz and Philips 2023).

CO and H_2 uptake parameters have also been fitted to literature data using a full model of the syngas fermentation (de Medeiros et al. 2019). This is challenging because data may be lacking to estimate the gas–liquid transfer with sufficient accuracy and hence the dissolved syngas concentrations.

To demonstrate the knowledge gap on dissolved syngas concentration, we used literature correlations to predict for $k_{L,}a$ of O_2 together with Eqs. (8)–(10) to predict dissolved CO concentrations from gas phase concentrations for steady states from Table 1 that use CO only. For details on the method, see Kerkhof (2024). The CO uptake rates given in Table 2 are plotted against the calculated dissolved CO concentration in Fig. 6. For comparison, Eq. (12) with the parameters of Mohammadi et al. (2014) is included. The lack of a pattern for the markers indicates that merely the order of magnitude of the dissolved CO concentration in the considered chemostat experiments is known.

Figure 6 shows $-q_{CO} = 69 \pm 6$ $mmol_{CO}/(g_X\ h)$ as the highest value for the reconciled chemostat data. This was achieved at pH 5 for a dilution rate of 0.116 h^{-1}, which is also the highest specific growth rate published for chemostats with *C. autoethanogenum* (de Lima 2022). As shown below, somewhat lower maximum specific growth rates have been measured in batch operation, such that one might assume that de Lima et al. (2022) operated close to washout and that $-q_{CO} = 69$ $mmol_{CO}/(g_X\ h)$ may have approached $-q_{CO}^{max}$. Allaart et al. (2023) calculated at pH 5.5 even $-q_{CO} = 119$ $mmol_{CO}/(g_X\ h)$ during CO pulses in a chemostat operation and assumed that $-q_{CO}^{max}$ had not yet been achieved. The value $-q_{CO}^{max} = 34.4$ $mmol_{CO}/(g_X\ h)$ for *C. ljungdahlii* from Table 3 is considerably lower.

Various μ values for batch growth of *C. autoethanogenum* have also been reported in literature. For batch growth of *C. autoethanogenum* on syngas (50% N_2, 20% CO, 20% CO_2 and 10% H_2) at pH 6.8 (uncontrolled) with mainly acetate production, Cotter et al. (2009) published data from which $\mu = 0.093$ h^{-1} was calculated from the exponential growth phase (Kerkhof 2024). Though, Oliveira et al. (2022) reported $\mu = 0.065$ h^{-1} for batch growth on syngas (60% CO, 20% CO_2 and 20% H_2) at pH 6 (controlled) with mainly ethanol production. Valgepea et al. (2017a) published a doubling time of 7.3 h for batch growth of *C. autoethanogenum* on syngas (29% N_2, 50% CO, 18% CO_2 and 3% H_2) at pH 5.7 with slight acetate production from which $\mu = 0.095$ h^{-1} was calculated.

For none of these batch values, it is sure if CO inhibition and limitation were both negligible such that μ can be assumed to be μ^{max}. In the most optimistic scenario, each μ equalled μ^{max}, and also de Lima et al. (2022) approached μ^{max} closely. Then, one can average the values from the aforementioned sources, which would lead to a provisional value of $\mu^{max} = 0.092 \pm 0.018$ h^{-1} for *C. autoethanogenum*.

Although these are questionable assumptions, this provisional value of μ^{max} can be used as μ in Eq. (7), leading

Table 3 Parameters determined for microbial CO uptake rate with Eq. (12)

Microbe	q_{CO}^{max} [$mmol_{CO}/(g_x\ h)$]	$K_{s,CO}$ [$mmol_{CO}/L$]	$K_{I,CO}$ [$mmol_{CO}/L$]	Source
Peptostreptococcus productus	− 144	0.016	> 12	Vega et al. (1989)
Eubacterium limosum	− 44.5	0.082	8.0	Chang et al. (2001)
C. ljungdahlii	− 34.4	0.017	0.50	Mohammadi et al. (2014)
C. aceticum	− 39 [a]	0.00025	0.07	Mayer et al. (2018)

[a]Recalculated from q_{AcT}^{max} using Eq. (3)

to crude estimates of 89% CO use for growth and 11% for maintenance during exponential growth. When evaluating the relation between growth rate and dissolved CO concentration by using Eq. (13) according to Monod with CO inhibition, this maintenance is neglected. It is recommended to use instead Eq. (12) with Eq. (7).

$$\mu = \mu^{max} \frac{c_{CO}}{K_{s,CO} + c_{CO} + \frac{(c_{CO})^2}{K_{I,CO}}} \tag{13}$$

Influence of acetic acid concentration

Increasing AcT concentrations will lead to increasing HAc concentrations, with the proportionality depending on pH according to the dissociation equilibria. The steady states of Table 1 cover a pH range of 5 to 6.2 and a c_{AcT} range of 11 to 190 mmol/L, leading to a calculated c_{HAc} range of 1 to 60 mmol/L. Since HAc causes decoupling of the proton motive force and ATP synthesis, m_{ATP} should be a function f of c_{HAc}, thus modifying Eq. (6) into:

$$q_{R1} Y_{ATP,R1} + q_{R2} Y_{ATP,R2} = \frac{1}{Y^{max}_{x/ATP}} \mu + m_{ATP,0} \cdot [1 + f(c_{HAc})] \tag{14}$$

Here, $m_{ATP,0}$ is the maintenance in the absence of HAc.

Introducing function f introduces at least one additional parameter. We fitted Eq. (14) including two fermentations but did not find a significantly improved fit according to an F-test ($p > 0.05$; see Kerkhof (2024)). So, there is no justification yet for introducing function f.

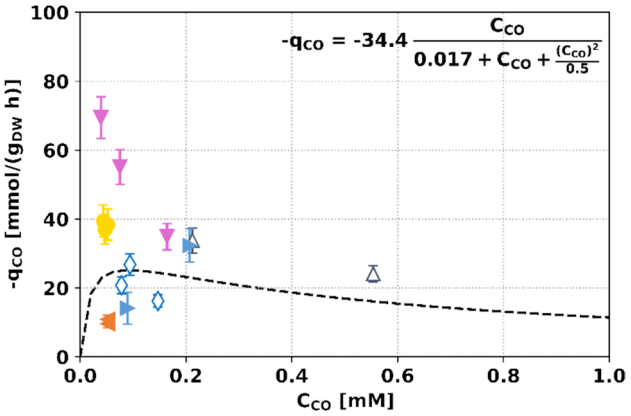

Fig. 6 CO uptake rates for fermentation by *C. autoethanogenum* as function of the dissolved CO concentrations. Line, simulation using Eq. (12) with kinetic parameters from Mohammadi et al. (2014). Markers, calculations from reconciliated experimental chemostat data: open triangle (Valgepea et al. 2018); diamond (Elisiário et al. 2023); circle (Chen et al. 2018); pink down arrow (de Lima et al. 2022); orange left arrow (Allaart 2023); blue right arrow (Diender 2019)

The rates of reactions R1 and R2 must depend on the concentrations of their substrates. R1 has only CO as substrate, whereas R2 has both CO and acetate as substrate. Suppose R1 and R2 would depend similarly on the CO concentration. This is a bold assumption. The equations below show a provisional hyperbolic dependence on c_{CO} and a hyperbolic dependence on c_{HAc}, the concentration of undissociated acetic acid.

$$q_{R1} = q^{max}_{R1} \frac{c_{CO}}{K_{CO} + c_{CO} + \frac{c^2_{CO}}{K_{i,CO}}} \tag{15}$$

$$q_{R2} = q^{max}_{R2} \frac{c_{CO}}{K_{CO} + c_{CO} + \frac{c^2_{CO}}{K_{i,CO}}} \cdot \frac{c_{HAc}}{K_{HAc} + c_{HAc}} \tag{16}$$

Now, in the ratio of these rates, the dependence on c_{CO} cancels out:

$$\frac{q_{R2}}{q_{R1}} = \frac{q^{max}_{R2}}{q^{max}_{R1}} \frac{c_{HAc}}{K_{HAc} + c_{HAc}} \tag{17}$$

Fitting Eq. (17) to the reconciled data yielded as fitted parameters $q^{max}_{R2}/q^{max}_{R1} = 1.64 \pm 1.26$ and $K_{HAc} = 91 \pm 101$ mmol/L. When using Eq. (17) with c_{AcT} instead of c_{HAc}, the fit became worse, because more ethanol is formed at lower pH, where the HAc/AcT ratio increases.

A threshold value of c_{HAc} required for R2 (Richter et al. 2016) might be seen in Fig. 7 from the very low values of q_{R2}/q_{R1} for $c_{HAc} < 10$ mmol/L.

However, the modest fit in Fig. 7 suggests that not only the acetic acid concentration influences the ratio q_{R2}/q_{R1}. For example, the dissolved CO concentration might influence q_{R1} and q_{R2} differently, because CO enters the metabolism at different enzymes. Besides, the large standard deviations in the fitted parameter values will also partly originate from the fact that $c_{HAc} < K_{HAc}$ for all data points. A good fit would need to include data for $c_{HAc} >> K_{HAc}$, but the used strain might not tolerate such values of c_{HAc}.

Although Eq. (17) and its fitted parameter values are tentative, their consequences can be calculated. Irrespective of the CO concentration, q_{R2} would reach q_{R1} if c_{HAc} would reach 142 mmol/L, which is when c_{AcT} would reach 389 mmol/L (23 g/L) in case of pH 5. Then, no net acetate production would be observed, because $q_{AcT} = q_{R1} - q_{R2}$, and only ethanol would be produced. Co-feeding of a chemostat with AcT would be required to get c_{AcT} at 23 g/L. Again, the microbe might not tolerate such a high concentration at pH 5.

To get a high selectivity of ethanol to acetate, H_2 may be required. Table 2 shows the highest values q_{EtOH}/q_{AcT}

and hence of q_{R2}/q_{R1} during H_2 consumption, but a deeper mechanistic and quantitative study of the product selectivity requires more data with H_2 supply. As CO inhibits hydrogenases and thus H_2 uptake (Mahamkali et al. 2020), increased knowledge of dissolved CO concentration is pertinent.

Influence of concentrations of ethanol and BDO

Ethanol inhibition of syngas fermentation has been studied for *C. carboxidivorans* by Fernández-Naveira et al. (2016). In batch bottles, growth on CO was measured during the early exponential phase, when mass transfer should not be limiting. The maximum growth rate μ^{max} decreased linearly from its base value μ_0^{max} when increasing amounts of ethanol were added initially. This is in line with Eq. (18), which is generally used to describe product inhibition by ethanol (Straathof 2023). The critical ethanol concentration for growth, $c_{EtOH}^{crit,\mu}$, was found to be 45 g/L by extrapolating the data of Fernández-Naveira et al. (2016).

$$\mu^{max} = \mu_0^{max}\left(1 - \frac{c_{EtOH}}{c_{EtOH}^{crit,\mu}}\right) \tag{18}$$

The maximum growth rate of *C. carboxidivorans* in the absence of ethanol was $0.086 \pm 0.004\ h^{-1}$ (Fernández-Naveira et al. 2016), which is comparable with the aforementioned values for *C. autoethanogenum* at similar conditions. We found no ethanol inhibition studies for the latter microbe, so the *C. carboxidivorans* data might be the best approximation. In a conventional chemostat, $c_{EtOH}^{crit,\mu}$ is the maximum achievable concentration. However, when cells are retained, or fed from an earlier stage, the achievable concentration is higher because these cells can still produce ethanol in reaction R2 to generate ATP for maintenance (Straathof 2023). Note that cell recycling with acetate recycling merely needs ethanol removal from the fermentation outflow by vacuum distillation (Janković et al. 2023).

BDO tolerance seems to be in the same range as ethanol tolerance. When adding increasing amounts of BDO to cultures of *C. autoethanogenum*, growth and acetate production ceased at 40 to 50 g/L (Köpke et al. 2011).

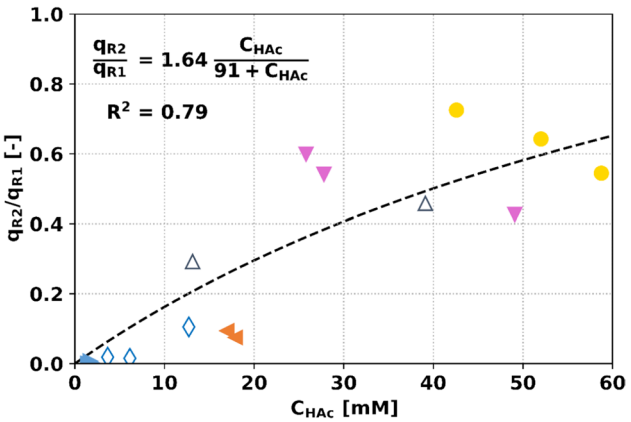

Fig. 7 The ratio of the catabolic reaction rates (q_{R2}/q_{R1}) plotted as a function of the undissociated acetic acid concentration (c_{HAc}). The line is the fit of Eq. (17) to the reconciliated experimental data: open triangle (Valgepea et al. 2018); diamond (Elisiário et al. 2023); circle (Chen et al. 2018); pink down arrow (de Lima et al. 2022); orange left arrow (Allaart 2023); blue right arrow (Diender 2019)

Conclusions

A considerable set of experimental *C. autoethanogenum* fermentation data is available. The chemostat data have been reconciled to improve their consistency. Most published chemostat experiments use CO without H_2. Biomass-specific rates from these CO experiments are related to each other according to simple reaction stoichiometries and the Pirt equation, with only the ratio of ethanol to acetate production remaining as degree of freedom. No straightforward dependency of this ratio on dissolved concentrations, such as CO or acetic acid concentration, was found. This is largely caused by the lack of knowledge about the dependency of the CO uptake rate (and hence all other rates) on the CO concentration. This knowledge gap is caused by a lack of dissolved CO measurements. For dissolved H_2, such a lack also applies. H_2 use adds unknown kinetic parameters, so much more experimental data with H_2 will be required. Moreover, more experiments with added products such as acetate and ethanol are needed to determine the influence of these products on the fermentation and its inhibition.

Overall, using basic kinetic equations has demonstrated knowledge gaps that cannot be filled by introducing additional equations that describe intracellular kinetics. When sufficient useful experimental data are available, more complex equations than treated here will be needed to describe the experiments. Although the focus of this review has been on *C. autoethanogenum*, most of the reasoning will be also applicable to gas fermentation by other microbes.

Supplementary Information The online version contains supplementary material available at https://doi.org/10.1007/s00253-024-13364-3.

Acknowledgements This study was funded by Delft University of Technology. The authors thank Eduardo Almeida Benalcázar for providing valuable input on analyzing the data, and Martijn Diender, Kaspar Valgepea, and James Heffernan for providing supplementary experimental data.

Author contribution IK and AS conceived the study and analyzed data. IK and LP and AS performed literature research and wrote the manuscript. All authors read and approved the manuscript.

Data Availability Not applicable.

Declarations

Ethical approval Not applicable.

Competing interests The authors declare no competing interests.

References

Allaart MT (2023) Poison to products: on harnessing the power of microorganisms to convert waste streams into new chemicals. PhD thesis, Delft University of Technology, https://doi.org/10.4233/uuid:bbf1eb72-9cc7-4e64-adf0-d869954c1750

Allaart MT, Diender M, Sousa DZ, Kleerebezem R (2023) Overflow metabolism at the thermodynamic limit of life: how carboxydotrophic acetogens mitigate carbon monoxide toxicity. Microb Biotechnol 16:697–705. https://doi.org/10.1111/1751-7915.14212

Almeida Benalcázar E, Noorman H, Maciel Filho R, Posada JA (2020) Modeling ethanol production through gas fermentation: a biothermodynamics and mass transfer-based hybrid model for microbial growth in a large-scale bubble column bioreactor. Biotechnol Biofuels 13:59. https://doi.org/10.1186/s13068-020-01695-y

Bachmann M, Völker S, Kleinekorte J, Bardow A (2023) Syngas from what? Comparative life-cycle assessment for syngas production from biomass, CO_2, and steel mill off-gases. ACS Sust Chem Eng 11:5356–5366. https://doi.org/10.1021/acssuschemeng.2c05390

Bae J, Song Y, Lee H, Shin J, Jin S, Kang S, Cho B-K (2022) Valorization of C1 gases to value-added chemicals using acetogenic biocatalysts. Chem Eng J 428:131325. https://doi.org/10.1016/j.cej.2021.131325

Chang IS, Kim BH, Lovitt RW, Bang JS (2001) Effect of CO partial pressure on cell-recycled continuous CO fermentation by *Eubacterium limosum* KIST612. Process Biochem 37:411–421. https://doi.org/10.1016/S0032-9592(01)00227-8

Chen B-Y, Chuang F-Y, Lin C-L, Chang J-S (2012) Deciphering butanol inhibition to Clostridial species in acclimatized sludge for improving biobutanol production. Biochem Eng J 69:100–105. https://doi.org/10.1016/j.bej.2012.09.005

Chen J, Daniell J, Griffin D, Li X, Henson MA (2018) Experimental testing of a spatiotemporal metabolic model for carbon monoxide fermentation with *Clostridium autoethanogenum*. Biochem Eng J 129:64–73. https://doi.org/10.1016/j.bej.2017.10.018

Cotter JL, Chinn MS, Grunden AM (2009) Influence of process parameters on growth of *Clostridium ljungdahlii* and *Clostridium autoethanogenum* on synthesis gas. Enzyme Microb Technol 44:281–288. https://doi.org/10.1016/j.enzmictec.2008.11.002

Dang J, Wang N, Atiyeh HK (2021) Review of dissolved CO and H_2 measurement methods for syngas fermentation. Sensors 21:2165

de Lima LA, Ingelman H, Brahmbhatt K, Reinmets K, Barry C, Harris A, Marcellin E, Köpke M, Valgepea K (2022) Faster growth enhances low carbon fuel and chemical production through gas fermentation. Front Bioeng Biotechnol 10 https://doi.org/10.3389/fbioe.2022.879578

de Medeiros EM, Posada JA, Noorman H, Filho RM (2019) Dynamic modeling of syngas fermentation in a continuous stirred-tank reactor: multi-response parameter estimation and process optimization. Biotechnol Bioeng 116:2473–2487. https://doi.org/10.1002/bit.27108

de Souza Pinto Lemgruber R, Valgepea K, Tappel R, Behrendorff JB, Palfreyman RW, Plan M, Hodson MP, Simpson SD, Nielsen LK, Köpke M, Marcellin E (2019) Systems-level engineering and characterisation of *Clostridium autoethanogenum* through heterologous production of poly-3-hydroxybutyrate (PHB). Metab Eng 53:14–23. https://doi.org/10.1016/j.ymben.2019.01.003

Detz R, Beerse M, Meulendijks N, Buskens P, van der Zwaan B (2024) Towards the use of renewable syngas for the decarbonization of industry. ChemSusChem:e202400059 https://doi.org/10.1002/cssc.202400059

Diender M (2019) Exploration of microbial systems as biocatalysts for conversion of synthesis gas to bio-based chemicals. PhD thesis, Wageningen University, https://doi.org/10.18174/466065

Dykstra JC, van Oort J, Yazdi AT, Vossen E, Patinios C, van der Oost J, Sousa DZ, Kengen SWM (2022) Metabolic engineering of *Clostridium autoethanogenum* for ethyl acetate production from CO. Microb Cell Fact 21:243. https://doi.org/10.1186/s12934-022-01964-5

Elisiário MP, De Wever H, Van Hecke W, Noorman H, Straathof AJJ (2022) Membrane bioreactors for syngas permeation and fermentation. Crit Rev Biotechnol 42:856–872. https://doi.org/10.1080/07388551.2021.1965952

Elisiário MP, Van Hecke W, De Wever H, Noorman H, Straathof AJJ (2023) Acetic acid, growth rate, and mass transfer govern shifts in CO metabolism of *Clostridium autoethanogenum*. Appl Microbiol Biotechnol 107:5329–5340. https://doi.org/10.1007/s00253-023-12670-6

Fackler N, Heijstra BD, Rasor BJ, Brown H, Martin J, Ni Z, Shebek KM, Rosin RR, Simpson SD, Tyo KE, Giannone RJ, Hettich RL, Tschaplinski TJ, Leang C, Brown SD, Jewett MC, Köpke M (2021) Stepping on the gas to a circular economy: accelerating development of carbon-negative chemical production from gas fermentation. Ann Rev Chem Biomolec Eng 12:439–470. https://doi.org/10.1146/annurev-chembioeng-120120-021122

Fernández-Blanco C, Robles-Iglesias R, Naveira-Pazos C, Veiga MC, Kennes C (2023) Production of biofuels from C1-gases with Clostridium and related bacteria—recent advances. Microb Biotechnol 16:726–741. https://doi.org/10.1111/1751-7915.14220

Fernández-Naveira Á, Abubackar HN, Veiga MC, Kennes C (2016) Carbon monoxide bioconversion to butanol-ethanol by *Clostridium carboxidivorans*: kinetics and toxicity of alcohols. Appl Microbiol Biotechnol 100:4231–4240. https://doi.org/10.1007/s00253-016-7389-8

Garcia-Ochoa F, Gomez E (2009) Bioreactor scale-up and oxygen transfer rate in microbial processes: an overview. Biotechnol Adv 27:153–176. https://doi.org/10.1016/j.biotechadv.2008.10.006

Heffernan JK, Valgepea K, de Souza Pinto Lemgruber R, Casini I, Plan M, Tappel R, Simpson SD, Köpke M, Nielsen LK, Marcellin E (2020) Enhancing CO_2-valorization using *Clostridium*

autoethanogenum for sustainable fuel and chemicals production. Front Bioeng Biotechnol 8 https://doi.org/10.3389/fbioe.2020.00204

Heijnen JJ, Kleerebezem R (2010) Bioenergetics of microbial growth. In: Flickinger MC (ed) Encyclopedia of industrial biotechnology, bioprocess, bioseparation, and cell technology, Volumes 1–7. John Wiley & Sons, pp 594–616

Heijnen JJ, Vanscheltinga AHT, Straathof AJ (1992) Fundamental bottlenecks in the application of continuous bioprocesses. J Biotechnol 22:3–20. https://doi.org/10.1016/0168-1656(92)90128-v

Ingelman H, Heffernan JK, Harris A, Brown SD, Shaikh KM, Saqib AY, Pinheiro MJ, de Lima LA, Martinez KR, Gonzalez-Garcia RA, Hawkins G, Daleiden J, Tran L, Zeleznik H, Jensen RO, Reynoso V, Schindel H, Jänes J, Simpson SD, Köpke M, Marcellin E, Valgepea K (2024) Autotrophic adaptive laboratory evolution of the acetogen *Clostridium autoethanogenum* delivers the gas-fermenting strain LAbrini with superior growth, products, and robustness. New Biotechnol 83:1–15. https://doi.org/10.1016/j.nbt.2024.06.002

Janković T, Straathof AJJ, Kiss AA (2023) Advanced downstream processing of bioethanol from syngas fermentation. Separ Purif Technol 322:124320. https://doi.org/10.1016/j.seppur.2023.124320

Katsyv A, Müller V (2020) Overcoming energetic barriers in acetogenic C1 conversion. Front Bioeng Biotechnol 8 https://doi.org/10.3389/fbioe.2020.621166

Kerkhof I (2024) Kinetic modelling of steady-state CO fermentation by *Clostridium autoethanogenum*. Master thesis, Delft University of Technology, http://resolver.tudelft.nl/uuid:dcb94ba6-343b-48fb-b432-d114352d2ade

Khalid H, Amin FR, Gao L, Chen L, Chen W, Javed S, Li D (2024) Syngas conversion to biofuels and biochemicals: a review of process engineering and mechanisms. Sust Ener Fuels 8:9–28

Kim J-Y, Lee M, Oh S, Kang B, Yasin M, Chang IS (2023) Acetogen and acetogenesis for biological syngas valorization. Biores Technol 384:129368. https://doi.org/10.1016/j.biortech.2023.129368

Köpke M, Gerth Monica L, Maddock Danielle J, Mueller Alexander P, Liew F, Simpson Séan D, Patrick Wayne M (2014) Reconstruction of an acetogenic 2,3-butanediol pathway involving a novel NADPH-dependent primary-secondary alcohol dehydrogenase. Appl Environ Microbiol 80:3394–3403. https://doi.org/10.1128/AEM.00301-14

Köpke M, Mihalcea C, Liew F, Tizard Joseph H, Ali Mohammed S, Conolly Joshua J, Al-Sinawi B, Simpson Séan D (2011) 2,3-Butanediol production by acetogenic bacteria, an alternative route to chemical synthesis, using industrial waste gas. Appl Environ Microbiol 77:5467–5475. https://doi.org/10.1128/AEM.00355-11

Köpke M, Simpson SD (2020) Pollution to products: recycling of 'above ground' carbon by gas fermentation. Curr Opin Biotechnol 65:180–189. https://doi.org/10.1016/j.copbio.2020.02.017

Lange HC, Heijnen JJ (2001) Statistical reconciliation of the elemental and molecular biomass composition of *Saccharomyces cerevisiae*. Biotechnol Bioeng 75:334–344. https://doi.org/10.1002/bit.10054

Liew F, Henstra AM, Köpke M, Winzer K, Simpson SD, Minton NP (2017) Metabolic engineering of *Clostridium autoethanogenum* for selective alcohol production. Metab Eng 40:104–114. https://doi.org/10.1016/j.ymben.2017.01.007

Liew F, Martin ME, Tappel RC, Heijstra BD, Mihalcea C, Köpke M (2016) Gas fermentation—a flexible platform for commercial scale production of low-carbon-fuels and chemicals from waste and renewable feedstocks. Front Microbiol 7 https://doi.org/10.3389/fmicb.2016.00694

Liew FE, Nogle R, Abdalla T, Rasor BJ, Canter C, Jensen RO, Wang L, Strutz J, Chirania P, De Tissera S, Mueller AP, Ruan Z, Gao A, Tran L, Engle NL, Bromley JC, Daniell J, Conrado R, Tschaplinski TJ, Giannone RJ, Hettich RL, Karim AS, Simpson SD, Brown SD, Leang C, Jewett MC, Köpke M (2022) Carbon-negative production of acetone and isopropanol by gas fermentation at industrial pilot scale. Nat Biotechnol 40:335–344. https://doi.org/10.1038/s41587-021-01195-w

Liu Z-Y, Jia D-C, Zhang K-D, Zhu H-F, Zhang Q, Jiang W-H, Gu Y, Li F-L (2020) Ethanol metabolism dynamics in *Clostridium ljungdahlii* grown on carbon monoxide. Appl Environ Microbiol 86:e00730-e820. https://doi.org/10.1128/AEM.00730-20

Ljungdhal LG (1986) The autotrophic pathway of acetate synthesis in acetogenic bacteria. Annu Rev Microbiol 40:415–450. https://doi.org/10.1146/annurev.mi.40.100186.002215

Mahamkali V, Valgepea K, de Souza Pinto Lemgruber R, Plan M, Tappel R, Köpke M, Simpson SD, Nielsen LK, Marcellin E (2020) Redox controls metabolic robustness in the gas-fermenting acetogen *Clostridium autoethanogenum*. PNAS 117:13168-13175. https://doi.org/10.1073/pnas.1919531117

Mann M, Miebach K, Büchs J (2021) Online measurement of dissolved carbon monoxide concentrations reveals critical operating conditions in gas fermentation experiments. Biotechnol Bioeng 118:253–264. https://doi.org/10.1002/bit.27567

Mayer A, Schädler T, Trunz S, Stelzer T, Weuster-Botz D (2018) Carbon monoxide conversion with *Clostridium aceticum*. Biotechnol Bioeng 115:2740–2750. https://doi.org/10.1002/bit.26808

Mock J, Zheng Y, Mueller AP, Ly S, Tran L, Segovia S, Nagaraju S, Köpke M, Dürre P, Thauer RK (2015) Energy conservation associated with ethanol formation from H_2 and CO_2 in *Clostridium autoethanogenum* involving electron bifurcation. J Bacteriol 197:2965–2980. https://doi.org/10.1128/jb.00399-15

Mohammadi M, Mohamed AR, Najafpour GD, Younesi H, Uzir MH (2014) Kinetic studies on fermentative production of biofuel from synthesis gas using *Clostridium ljungdahlii*. Sci World J 2014:910590. https://doi.org/10.1155/2014/910590

Morinaga T, Kawada N (1990) The production of acetic acid from carbon dioxide and hydrogen by an anaerobic bacterium. J Biotechnol 14:187–194. https://doi.org/10.1016/0168-1656(90)90007-X

Munasinghe PC, Khanal SK (2014) Evaluation of hydrogen and carbon monoxide mass transfer and a correlation between the myoglobin-protein bioassay and gas chromatography method for carbon monoxide determination. RSC Adv 4:37575–37581. https://doi.org/10.1039/C4RA04696J

Munoz L, Philips J (2023) No acetogen is equal: strongly different H_2 thresholds reflect diverse bioenergetics in acetogenic bacteria. Environ Microbiol 25:2032–2040. https://doi.org/10.1111/1462-2920.16429

Norman ROJ, Millat T, Schatschneider S, Henstra AM, Breitkopf R, Pander B, Annan FJ, Piatek P, Hartman HB, Poolman MG, Fell DA, Winzer K, Minton NP, Hodgman C (2019) Genome-scale model of *C. autoethanogenum* reveals optimal bioprocess conditions for high-value chemical production from carbon monoxide. Eng Biol 3:32–40. https://doi.org/10.1049/enb.2018.5003

Oliveira L, Rückel A, Nordgauer L, Schlumprecht P, Hutter E, Weuster-Botz D (2022) Comparison of syngas-fermenting clostridia in stirred-tank bioreactors and the effects of varying syngas impurities. Microorganisms 10:681

Owoade A, Alshami AS, Levin D, Onaizi S, Malaibari ZO (2023) Progress and development of syngas fermentation processes toward commercial bioethanol production. Biofuels Bioprod Biorefin 17:1328–1342. https://doi.org/10.1002/bbb.2481

Perret L, Boukis N, Sauer J (2024) Synthesis gas fermentation at high cell density: how pH and hydrogen partial pressure affect productivity and product ratio in continuous fermentation. Bioresour Technol 391:129894. https://doi.org/10.1016/j.biortech.2023.129894

Pirt SJ (1965) The maintenance energy of bacteria in growing cultures. Proc R Soc Lond B 163:224–231. https://doi.org/10.1098/rspb.1965.0069

Puiman L, Almeida Benalcázar E, Picioreanu C, Noorman HJ, Haringa C (2024) High-resolution computation predicts that low dissolved CO concentrations and CO gradients promote ethanol production at industrial-scale gas fermentation. Biochem Eng J 207:109330. https://doi.org/10.1016/j.bej.2024.109330

Puiman L, Elisiário MP, Crasborn LML, Wagenaar LECH, Straathof AJJ, Haringa C (2022) Gas mass transfer in syngas fermentation broths is enhanced by ethanol. Biochem Eng J 185:108505. https://doi.org/10.1016/j.bej.2022.108505

Richter H, Martin ME, Angenent LT (2013) A two-stage continuous fermentation system for conversion of syngas into ethanol Energies. vol 6, p 3987-4000

Richter H, Molitor B, Wei H, Chen W, Aristilde L, Angenent LT (2016) Ethanol production in syngas-fermenting *Clostridium ljungdahlii* is controlled by thermodynamics rather than by enzyme expression. Ener Environ Sci 9:2392–2399. https://doi.org/10.1039/C6EE01108J

Schuchmann K, Müller V (2014) Autotrophy at the thermodynamic limit of life: a model for energy conservation in acetogenic bacteria. Nature Rev Microbiol 12:809–821. https://doi.org/10.1038/nrmicro3365

Stoll IK, Boukis N, Sauer J (2020) Syngas fermentation to alcohols: reactor technology and application perspective. Chem Ing Techn 92:125–136. https://doi.org/10.1002/cite.201900118

Straathof AJJ (2023) Modelling of end-product inhibition in fermentation. Biochem Eng J 191:108796. https://doi.org/10.1016/j.bej.2022.108796

Sun X, Atiyeh HK, Huhnke RL, Tanner RS (2019) Syngas fermentation process development for production of biofuels and chemicals: a review. Biores Technol Rep 7:100279. https://doi.org/10.1016/j.biteb.2019.100279

Ungerman AJ, Heindel TJ (2007) Carbon monoxide mass transfer for syngas fermentation in a stirred tank reactor with dual impeller configurations. Biotechnol Prog 23:613–620. https://doi.org/10.1021/bp060311z

Valgepea K, de Souza Pinto Lemgruber R, Abdalla T, Binos S, Takemori N, Takemori A, Tanaka Y, Tappel R, Köpke M, Simpson SD, Nielsen LK, Marcellin E (2018) H_2 drives metabolic rearrangements in gas-fermenting *Clostridium autoethanogenum*. Biotechnol Biofuels 11:55https://doi.org/10.1186/s13068-018-1052-9

Valgepea K, de Souza Pinto Lemgruber R, Meaghan K, Palfreyman RW, Abdalla T, Heijstra BD, Behrendorff JB, Tappel R, Köpke M, Simpson SD, Nielsen LK, Marcellin E (2017a) Maintenance of ATP homeostasis triggers metabolic shifts in gas-fermenting acetogens. Cell Syst 4:505-515.e5 https://doi.org/10.1016/j.cels.2017.04.008

Valgepea K, Loi KQ, Behrendorff JB, Lemgruber RdSP, Plan M, Hodson MP, Köpke M, Nielsen LK, Marcellin E (2017) Arginine deiminase pathway provides ATP and boosts growth of the gas-fermenting acetogen *Clostridium autoethanogenum*. Metab Eng 41:202–211. https://doi.org/10.1016/j.ymben.2017.04.007

van 't Riet K, Tramper J (1991) Basic bioreactor design. Marcel Dekker, New York

van Rosmalen RP, Martins dos Santos VAP, Suarez-Diez M (2022) Questions, data and models underpinning metabolic engineering. Front Syst Biol 2 https://doi.org/10.3389/fsysb.2022.998048

Vega JL, Clausen EC, Gaddy JL (1989) Study of gaseous substrate fermentations: carbon monoxide conversion to acetate. 1. Batch Culture Biotechnol Bioeng 34:774–784. https://doi.org/10.1002/bit.260340607

Volger R, Puiman L, Haringa C (2024) Bubbles and Broth: a review on the impact of broth composition on bubble column bioreactor hydrodynamics. Biochem Eng J 201:109124. https://doi.org/10.1016/j.bej.2023.109124

Wang S, Huang H, Kahnt J, Mueller AP, Köpke M, Thauer RK (2013) NADP-specific electron-bifurcating [FeFe]-hydrogenase in a functional complex with formate dehydrogenase in *Clostridium autoethanogenum* grown on CO. J Bacteriol 195:4373–4386. https://doi.org/10.1128/jb.00678-13

Whang K, Shin Y, Baek W, Jo Y, Hwang JH, Min J, Kim D, Kang T (2022) Direct and precise determination of volumetric mass transfer coefficient of carbon monoxide for miniaturized gas-liquid reactors via sensitive probing of raman transitions. Chem Eng J 429:132260. https://doi.org/10.1016/j.cej.2021.132260

Wood HG (1991) Life with CO or CO_2 and H_2 as a source of carbon and energy. FASEB J 5:156–163. https://doi.org/10.1096/fasebj.5.2.1900793

Yang C, Dong L, Gao Y, Jia P, Diao Q (2021) Engineering acetogens for biofuel production: from cellular biology to process improvement. Renew Sust Ener Rev 151:111563. https://doi.org/10.1016/j.rser.2021.111563